Electronic Supplementary Material (ESI) for Nanoscale Advances.


# Electronic Supporting Information

# pH-responded Hollow Fe–Gallic Acid Coordination Polymer for Multimodal Synergistic-therapy and MRI of Cancer

Congcong Liu,[1] Chengcheng Li, [1] Sen Jiang, [1] Cheng Zhang,[2] and Yang Tian[1*]

[1]Department of Chemistry, Analytical Instrumentation Center, 105 North Road of Western Third Ring, Haidian District, Beijing 100048, China

[2]College of Life Science, Capital Normal University, 105 North Road of Western Third Ring, Haidian District, Beijing 100048, China

Corresponding Author: Yang Tian

Email address: tianyang@cnu.edu.cn

## 1. Materials

Gallic acid ($C_7H_6O_5$), iron (III) chloride hexahydrate ($FeCl_3 \cdot 6H_2O$, ACS), Adriamycin (DOX), and polyvinylpyrrolidone (PVP) were purchased from Aladdin Chemical (Shanghai, China). Bovine serum albumin (BSA) was purchased from AMRESCO. Hydrogen peroxide ($H_2O_2$), ethanol, and concentrated sulfuric acid were purchased from Beijing Chemical Reagent Company (Beijing, China). The reduced glutathione kit was provided by Suzhou Keming Biotechnology Co., Ltd. Glutathione (GSH) and Rhodamine B (RhB) were supplied by Aladdin Biochemical Technology Co., Ltd. All other chemicals and reagents used in the experiments were of analytical purity grade and were not further processed before use. The resistivity of deionized water used in all experiments was higher than 18 MΩ $cm^{-17}$.

The cells we used in the experimental part were purchased from the Concordia Cell Resource Center (Beijing).C6 (rat glioma cells) is a rat glioma clone induced by Benda et al. with N-nitrosomethylurea and built after a series of in vitro cultures and animal passaging alternations. The resource number for C6 cells is 1101RAT-PUMC000131. HKC (human renal tubular epithelial cells) cells are of human origin and are commonly used in studies of renal tubular epithelial cell metabolism. The resource number of HKC is 1101HUM-PUMC000160.PC-12 [PC12] is a rat adrenal pheochromocytoma cell. The cell line is derived from adrenal pheochromocytoma of transplantable male rats; the resource number for PC-12 is 1101RAT-PUMC000024.HeLa (human cervical cancer cells) is of human origin. HeLa was the first aneuploid epithelial-like cell line obtained from human tissue in continuous culture, and it was established by Gey GO et al. in 1951 from cervical cancer tissue of a 31-year-old black woman. the resource number for HeLa is 1101HUM-

PUMC000011.293 [HEK-293] is a human embryonic kidney cell. The cell genome contains DNA from the left end of the adenovirus 5 (Ad5) genome. this cell is a host for human adenovirus vector amplification. the resource number for 293 is 1101HUM-PUMC000010.

## 2. Experimental Section

### 2.1 Synthesis of hollow nanospheres of Fe-GA/BSA

Polyethylene polyvinylpyrrolidone (PVP) of 15 mg was dissolved in 2 mL deionized water with magnetic stirring for 10 minutes. Then we added 33.3 mg bovine serum albumin (BSA) to the above solution and continued stirring for 10 minutes. The 2 mL $FeCl_3 \cdot 6H_2O$ solution (160 mM) was added dropwise to the above solution and stirred for 30 min to obtain a homogeneous solution. Then 2 mL GA solution (160 mM) was added to it in the same way. The reaction was carried out under ice-water bath conditions for 90 min. The obtained product was centrifuged at 8000 rpm and washed several times with deionized water.

### 2.2 Synthesis of the Fe-GA/BSA loaded with DOX (Fe-GA/BSA @DOX)

The 7 mg Fe-GA/BSA was dispersed in 6 mL deionized water with 1.5 mg DOX at room temperature with magnetic stirring for 24 h. The product obtained was centrifuged at 8000 rpm and washed with deionized water. 1.5 mg of DOX was dispersed in 6 ml of PBS solution, and the UV absorption value at 480 nm was measured. Then, the 6 mL PBS solution of Fe-GA/BSA (7 mg) was mixed with DOX solution (1.5 mg, 0.25 mg mL-1), and the supernatant was monitored by UV-vis absorption at different time points. The UV absorption value at 480 nm was used to establish a linear relationship with the concentration of DOX in the supernatant to calculate the mass of DOX loaded in Fe-GA/BSA.

**2.3 Release of DOX**

The prepared Fe-GA/BSA@DOX of 2 mg was tested in three different solutions: 2 mL PBS solution of pH=7.4, 2 mL PBS solution of pH=5.5, and 2 mL PBS solution of pH=5.5 with GSH (0.02 mg). The supernatant was extracted after release of 24 hours by centrifugation. The absorbance value of the supernatant at 480 nm was detected by a UV-*vis* spectrophotometer.

**2.4 In vitro photothermal performance test**

The Fe-GA/BSA@DOX of 2 mL were prepared with the concentrations of 0, 0.125, 0.25, 0.5, and 1 $mg \cdot mL^{-1}$ in an ampoule (5 mL). Fe-GA/BSA aqueous solution of 2 mL at the concentration of 1 $mg \cdot mL^{-1}$ were also prepared for use. The samples were then irradiated with a NIR laser of 808 nm and a power density of 0.7 $W \cdot cm^{-2}$ (MDL-III-808/1-2500 Mw). The other end of the laser was connected to a NIR thermal imager. The temperature change data and photothermal photos of the samples were obtained by the NIR thermal imager. The irradiation time for each group was 10 min, and the data was taken every 30 seconds. To calculate the photothermal conversion efficiency, the sample solution with a concentration of 1 $mg \cdot mL^{-1}$ was subjected to five heating and cooling cycles, and the data was still collected every 30 seconds.

**2.5 In vitro MR weighted imaging and relaxation rate assay**

Fe-GA/BSA@DOX aqueous solutions with iron ion concentrations of 0, 0.06, 0.125, 0.25, 0.5, and 1 $mg \cdot mL^{-1}$ were prepared for use. MR weighted imaging and relaxation time assays were performed on an MRI imager (MesoMR-60) with a magnetic field strength of 0.47 T.

The parameters were set as follows.

$T_1$-weighted MR images: TR = 500 ms, TE = 20 ms, FA = 176.57, matrix = 256 × 256, FOV = 4.0 × 4.0 $cm^2$, and slice thickness = 1 mm;

$T_2$-weighted MR images: TR = 3000 ms, TE = 45 ms, FA = 180, matrix = 256 × 256, FOV = 4.0 × 4.0 $cm^2$, and slice thickness = 1 mm.

The curve of relaxation time with Fe concentration was calculated by the formula:

$$1/T_i = 1/T_{i0} + r_i [M] \ (i = 1, 2)$$

Where $T_i$ is the $T_1$ or $T_2$ relaxation time in the presence of Fe-GA/BSA@DOX, $T_{i0}$ is the relaxation time of pure water, [M] is the concentration of iron in the contrast agent and $r_i$ is the rate of proton relaxation.

**2.6 Cell culture**

Cervical cancer cell line (HeLa cells) and rat adrenal medullary pheochromocytoma (PC-12 cells) were cultured in DMEM medium with 10% fetal bovine serum (FBS), penicillin (100 U·mL-1) and streptomyces (100 g·mL-1) at 37 °C and 5% CO2. Mouse glioma cells (C6 cells) were cultured in an F10 medium with horse serum (HS). Human embryonic kidney epithelial cells (HKC cells) were cultured in an F12 medium with 10% double-antibody, Human embryonic kidney cells (293 cells) were cultured in basal medium containing 8% DMSO and 20% FBS, and other conditions were kept constant.

**2.7 MTT assay**

Well-grown mouse glioma cells (C6), cervical cancer cell line (Hela), Human embryonic kidney cells (293 cells), rat adrenal medullary pheochromocytoma (PC-12 cells), and renal tubular epithelial cells (HKC) were inoculated into 96-well plates ($1 \times 10^4$ cells per well) and incubate at 37 °C with 100% humidity and 5% $CO_2$ concentration. PBS and different concentrations (62.5, 125, 250, 500 μg·$mL^{-1}$) of Fe-GA/BSA@DOX

materials were added to the wells, and the cells adhered to the well walls after 12 and 24 hours. Then, thiazole blue (MTT) was added to the wells for 4 h. Finally, dimethyl sulfoxide (DMSO) was added to the wells for 30 min in the dark. A microplate reader was used to detect the absorbance of each well at 570 nm.

The following formula was utilized to calculate the cell survival rate:

Cell viability (%) = (mean of absorbance values in the treatment group/mean of absorbance values in the control group) ×100.

**2.8 Fluorescence assay**

Well-grown mouse glioma cells (C6) were inoculated into 96-well plates ($1 \times 10^4$ cells per well), which were then placed in a constant temperature incubator at 37 °C with 100% humidity and 5% $CO_2$ concentration. PBS and Fe-GA/BSA@DOX material with the concentration of 1000 $\mu g \cdot mL^{-1}$ were added to the wells and cultured for 12 h. rhodamine 123 dye solution of 5 $\mu g \cdot mL^{-1}$ was added into the above solution. Then the solution was incubated in the incubator for 10 min. The cells were centrifuged and washed twice with a culture solution. The fluorescent signal of the stained cells was detected immediately using a fluorescent microscope.

**2.9 Determination of GSH content in cells**

C6 cells were seeded in 96 wells plate at a density of $1 \times 10^4$ cells per well and cultured at 37 °C for 24 h in 5% $CO_2$. Afterward, we measured the absorbance of the complex formed by DTNB and GSH at 412 nm according to the instructions of the GSH kit.

**2.10 MRI imaging in vivo**

Glioma-bearing mice were injected with 200 μL Fe-GA/BSA@DOX aqueous solution (1 $mg \cdot mL^{-1}$) through the tail vein. The MRI system was used to detect and record

the $T_1$ and $T_2$ signals before the injection and post-injection of 0.5, 1, 3, 5, and 24 h. The TR and TE parameters were the same as the in vitro tests. All animal procedures were performed in accordance with the Guidelines for Care and Use of Laboratory Animals of Capital Normal University and experiments were approved by the Animal Ethics Committee of Capital Normal University. The permit number is "IACUC NO.2021021".

**2.11 Photothermal conversion in vivo**

Glioma-bearing mice were injected with 200 uL of Fe-GA/BSA@DOX (1 $mg \cdot mL^{-1}$), Fe-GA/BSA (1 $mg \cdot mL^{-1}$), and PBS (1 $mg \cdot mL^{-1}$) solution. Then a NIR laser (MDL-III-808/1-2500Mw) with a wavelength of 808 nm and a power density of 0.7 $W \cdot cm^{-2}$ was used to irradiate the tumors in the mice for 10 min. The other end of the laser was used for NIR thermal imager connection. The temperature change data and photothermal photographs of the tumor site were obtained by the NIR thermographer every 30 seconds.

**2.12 Combination therapy in vivo**

Tumor-bearing mice (tumor volume ~100 $mm^3$, ICR mice) were divided into 6 groups: PBS, Fe-GA/BSA, Fe-GA/BSA @DOX, PBS+NIR, Fe-GA/BSA +NIR, Fe-GA/BSA @DOX+NIR. The concentrations of Fe-GA/BSA and Fe-GA/BSA@DOX were both 1 $mg \cdot mL^{-1}$, and the injection volume was 200 μL. The growth status, body weight, and the tumor volume of the mice were recorded every two days and continuously monitored for 20 days.

The tumor volume was calculated by the formula: $V_{tumor} = (a \times b^2)/2$

Where a is the length of the tumor and b is the width of the tumor.

**2.13 Histological analysis of living organisms**

After 20 days of continuous monitoring, the mice were sacrificed and dissected. The

mice's fresh organs were fixed with 4% neutral buffered formalin tissue fixative and then processed with paraffin. Tissue sections were stained with hematoxylin and eosin (H&E). Optical micrographs of the tissue sections were preserved.

## 3. Tables and figures

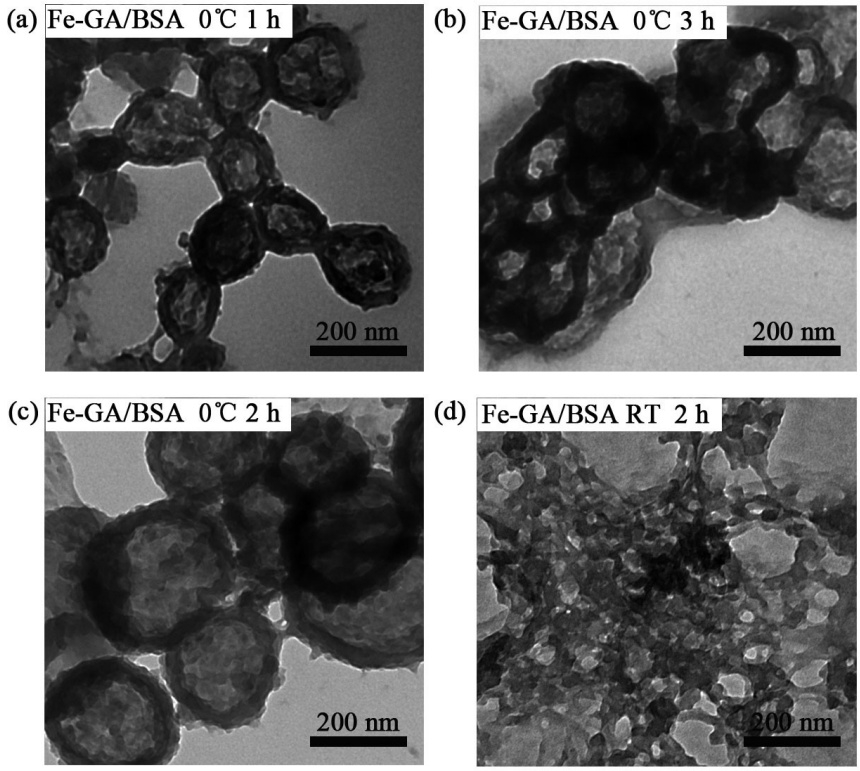


**Figure S1**. TEM images of Fe-GA/BSA synthesized under different reaction temperatures and reaction times.

In order to obtain ideal hollow Fe-GA/BSA spheres, we tried to prepare hollow Fe-GA/BSA nanospheres under different reaction conditions. Different products were obtained by adjusting the temperature and time of the reaction based on the fixed Fe (III) to GA molar ratio of 1:1, which were observed by TEM. Figure S1a-S1c were the TEM images of the effect of reaction time on the morphology of the products at 0 °C. Only when the reaction time was controlled for 2 h, the hollow structure with uniform morphology

was obtained, and the size of the hollow nanospheres was around 300 nm. Figure S1d indicates that the product obtained at room temperature with the same reaction time did not have regular morphology, which may be due to fast coordinating between Fe (III) and GA.

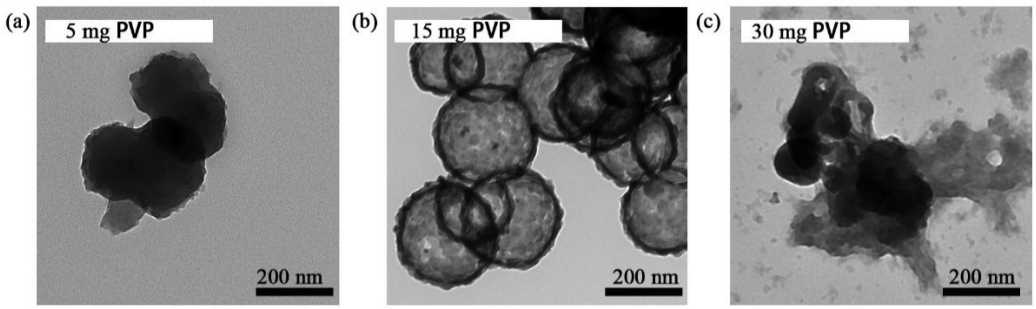


**Figure S2.** TEM images of the synthesized Fe-GA/BSA at different surfactant PVP contents

Based on the optimal reaction time and temperature, the effect of the amount of surfactant on its hollow structure was investigated. Figure S2 shows the morphological characteristics of the materials obtained under different surfactant contents. Figure S2a indicates the non-spherical particles obtained with 5 mg polyvinylpyrrolidone (PVP), and S2c shows the irregular aggregated particles obtained with 30 mg PVP. Figure S2b shows that when the PVP content was 15 mg, the final product was hollow spheres with uniform size.

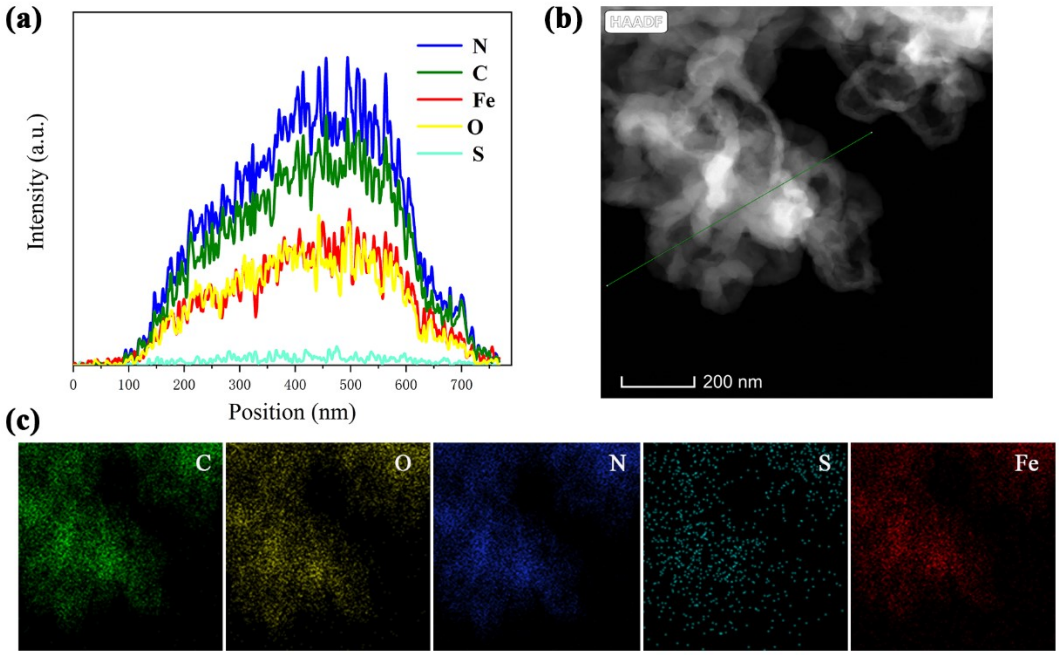


**Figure S3**. EELS line scan on the hollow nanospheres (a) and (b); elemental mapping (c) (green: C; Yellow: O; blue: N; blue-green: S; red: Fe)

As shown in Fig. S3, the elemental distribution of the hollow spheres was characterized by using a high-angle annular dark-field scanning transmission electron microscope (HADDF-STEM-EDS) and Electron Energy Loss Spectroscopy (EELS), which show the uniform distribution of the compositional elements.

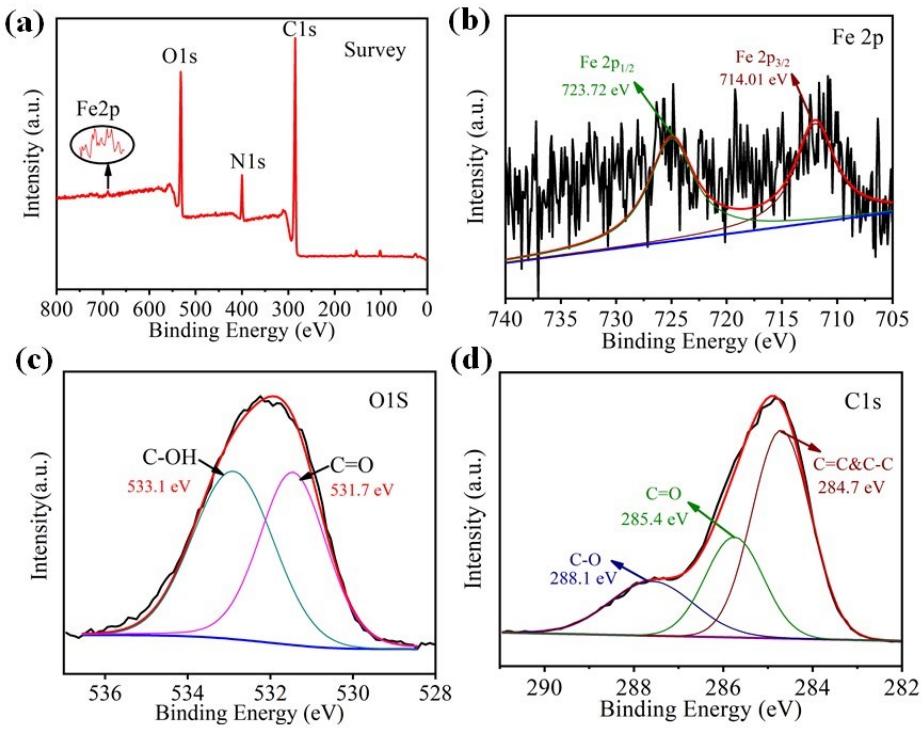


**Figure S4.** XPS spectra of the hollow Fe-GA/BSA nanospheres. Survey patterns (a); HR-XPS patterns of Fe 2p orbitals (b); O 1s orbitals (c) and C 1s orbitals (d)

Subsequently, we used X-ray photoelectron spectroscopy (XPS) to detect the material composition and determined the surface electronic state of the Fe-GA/BSA. As shown in Fig. S4a, the XPS survey spectrum of the sample shows the peaks of Fe, C, N, and O, consistent with expectations. Fig. S4b shows the HR-XPS spectrum of Fe 2p orbitals in the prepared Fe-GA/BSA. There are two characteristic peaks at 723.72 eV and 714.01 eV, which correspond to the orbitals of Fe $2p_{1/2}$ and Fe $2p_{3/2}$, respectively. [1, 2] In addition, the O 1s peaks at about 533.1 eV and 531.7 eV in Fig.S4c can be regarded as the characteristic peaks of C-O and C=O in carboxyl in Fe-GA and BSA. [3] In Fig.S4d, the C1s peak of 284.7eV is attributed to C-C and C=C in the organic composition of the sample, while the peaks of 285.4eV and 288.1eV corresponded to the carboxyl C=O and C-O in BSA and GA, respectively.

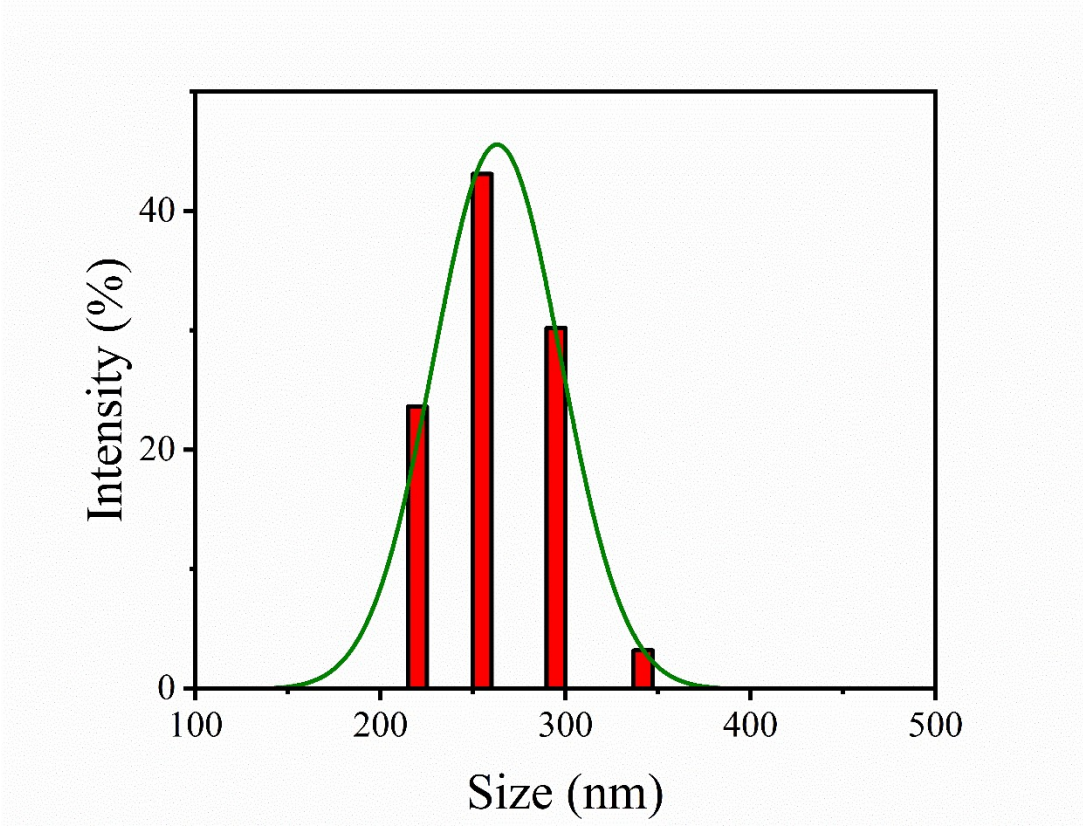


**Figure S5.** hydraulic dynamics size of the Fe-GA/BSA in PBS (pH=7.4)

**Table S1.** loading efficiency/encapsulation rate of some reported nanomaterials

| Nanocarrier material | Drug | Encapsulation efficiency (%) | Refs |
|---|---|---|---|
| PCN-Fe(III)-PTX nanoparticles | PTX | 47.3[4] | Ref. 2 |
| PCL/Fe3O4-DOX microspheres | DOX | 25.8[5] | Ref. 3 |
| DSPE-b-PEG-b-PAE-b-PEG-b-DSPE | DOX | 60.4 | Ref. 4 |
| Fe-GA/BSA@DOX | DOX | 66.1% | **This work** |

**Calculation of loading efficiency/encapsulation rate of DOX in Fe-GA/BSA**

$$Drug\ loading = \frac{mass\ of\ the\ drug}{total\ mass\ of\ the\ drug\ loaded\ nanoparticles} = \frac{W\ drug}{W\ drug\ +\ W\ nanocarrier} \quad (1)$$

$$Encapsulation\ efficiency = \frac{weight\ of\ the\ drug\ in\ nanoparticles}{weight\ of\ drug\ added} = \frac{W\ drug\ in\ nanoparticles}{W\ drug\ added} \quad (2)$$

DOX has a certain light absorption in the UV region, with an absorption peak at 480 nm. The light absorption standard curve of DOX can be established by UV absorbance. This method can be applied to detect the encapsulation rate of nanomaterials on DOX, the drug loading and in vitro release assay. The loading of DOX in Fe-GA/BSA@DOX was

analyzed as follows. Firstly, 1.5 mg of DOX was dispersed in 6 ml of PBS solution, and the UV absorption value at 480 nm was measured. Secondly, the 6 mL PBS solution of Fe-GA/BSA (7 mg) was mixed with DOX solution (1.5 mg, 0.25 mg mL-1), and the supernatant was monitored by UV-vis absorption at different time points. The UV absorption value at 480 nm was used to establish a linear relationship with the concentration of DOX in the supernatant to calculate the mass of DOX loaded in Fe-GA/BSA. Finally, the maximum value was calculated at 24 h by using the above equation.[6] The drug loading efficiency of DOX was 14.18%, and the encapsulation efficiency of DOX was 66.1%. The relevant calculation process has been detailed in the supporting information

| Materials | Near-infrared wavelength | power densities | the photothermal conversion efficiency | Refs |
|---|---|---|---|---|
| $Fe@Fe_3O_4$ | 808 nm | 1.0 W/cm$^2$ | 25.4%[7] | Ref. 5 |
| $Fe_3O_4$@PDA NCs | 808 nm | 0.9 W /cm$^2$ | 36% | Ref. 6 |
| HA-Fe-PAP | 808 nm | 1.0 W /cm$^2$ | 43.8% | Ref. 7 |
| PS@CS@Au–$Fe_3O_4$–FA/ICG | 980 nm | 0.6 W/cm$^2$ | 16% | Ref. 8 |
| $Fe_3O_4$@$Cu_2$−xS | 808 nm | 0.6 W/cm$^2$ | 27.7% | Ref. 9 |
| PLNP-GNR | 635 nm | 0.35W/cm$^2$ | 37% | Ref. 10 |
| $MoS_2$:5%$Eu^{3+}$ nanoflowers | 808 nm | 0.6 W/ cm$^2$ | 27.7% | Ref. 11 |
| Fe-GA/BSA@DOX | 808 nm | 0.7W /cm$^2$ | **67.14%** | **This work** |

**Table S2.** Photothermal conversion efficiency of some reported iron-based nanomaterials

**Calculation of photothermal conversion efficiency:**

$$\eta=\frac{hA\Delta T_{max}-Q_s}{I(1-10^{-A\lambda})} \quad (1)$$

$$hA=\frac{mC_p}{\tau} \quad (2)$$

The photothermal conversion efficiency η was calculated according to equation (1),

where η is the photothermal conversion efficiency; h is the heat transfer coefficient; A is the heated area of the sample; ΔT max is the maximum temperature difference; $Q_s$ is the heat value related to the absorbance of the solvent, which is measured here with pure water; I is the power density value of the excitation light; the laser with a power density of 0.7 W $cm^{-2}$ was used in this experiment; A λ is the near-infrared light absorption value of Fe-GA/BSA@DOX at a wavelength of 808 nm. h A is calculated from equation (2), where m is the mass of ultrapure water as a solvent (g), Cp is the specific heat capacity of water (4.2 J/g), τ is obtained from the temperature decay curve after removing the laser, with time as the vertical coordinate and -Ln(θ) as the horizontal coordinate, the calculated value of τ is 534.8, and the value of h is obtained by substituting this value into equation (2). The resulted photothermal conversion efficiency η was 67.14%.

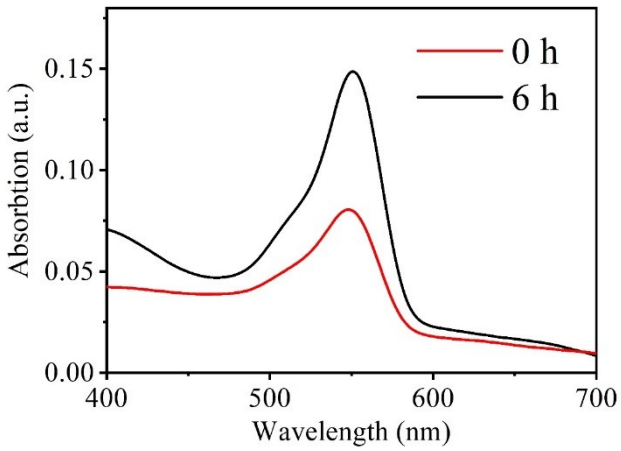


**Figure S6.** UV absorptions of the supernatant of Fe-GA /BSA mixed with RhB at 0 h and 6 h.

The ·OH content generated by the Fenton reaction was further evaluated by degrading RhB solution with Fe-GA/BSA, $H_2O_2$, and GSH mixing. The RhB content was monitored via the characteristic UV absorption peak of RhB around 554 nm. As shown in Figure S3, the results showed that the absorption peak at 554 nm decreased, and the degradation rate reached 63% after 6 h. This confirmed the Fe-GA/BSA could react with high concentrations GSH in the simulated tumor microenvironment and be used as a CDT agent.

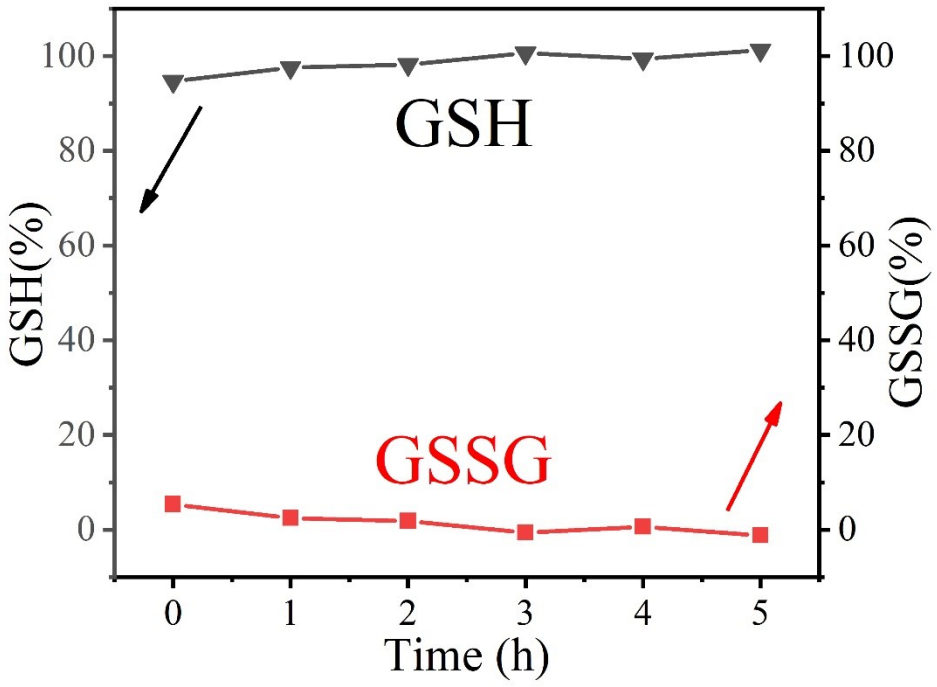


**Figure S7.** Detection of GSH and GSSG in the mixed solution of DOX and GSH.

We tested the GSH solution mixed with DOX instead of Fe-GA/BSA, as shown in Figure S4. It shows that the reduced GSH content did not decrease, and the oxidized glutathione content (GSSG) did not increase without Fe-GA/BSA in the solution.

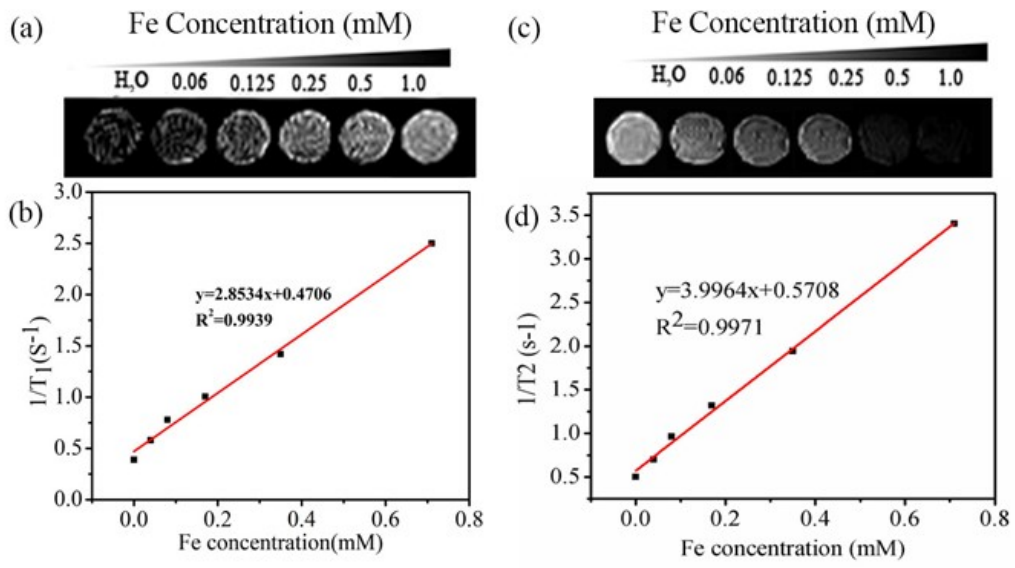


**Figure S8.** $T_1$-weighted (a) and $T_2$-wegihted (c) images of the Fe-GA/BSA@DOX at different concentrations; Relaxation rates $1/T_1$ (b) and $1/T_2$ (d) of Fe-GA/BSA@DOX.

In order to explore the effect of Fe-GA/BSA@DOX nanospheres as MRI contrast agents, we dispersed Fe-GA/BSA@DOX in water to obtain solutions with different Fe concentrations of 0.0625, 0.125, 0.25, 0.5, and 1 mM, respectively. The concentration of the Fe element was determined by ICP-MS. Figure S5a shows the $T_1$-weighted images of the solutions, which brightened as the Fe concentration increasing. Figure S5c shows the $T_2$-weighted images of the solutions, which darkened as the concentration increasing. Then, the $T_1$ and $T_2$ relaxation rates of Fe-GA/BSA@DOX were further calculated according to Figures S5b and S5d. The calculated values of relaxation ratio were $r_1$ = 2.8534 $mM^{-1} \cdot s^{-1}$ and $r_2$ = 3.9964 $mM^{-1} \cdot s^{-1}$, respectively.

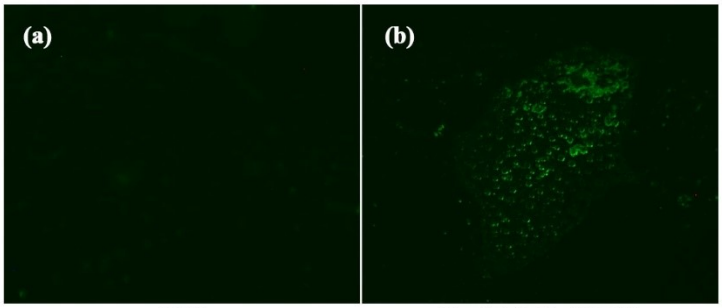


**Figure S9.** Fluorescence imaging of C6 cells with rhodamine 123 dyeing cultured with PBS and Fe-GA/BSA@DOX, respectively

Figure S6a suggests that the fluorescence signal of the control cells without Fe-GA/BSA@DOX treatment nearly faded. In contrast, Figure S6b displays that the cells after co-culture with the Fe-GA/BSA@DOX showed strong yellow-green fluorescence due to Rhodamine 123 re-releasing from the mitochondria. The results fully demonstrate that the Fe-GA/BSA@DOX has a killing effect on cancer cells.

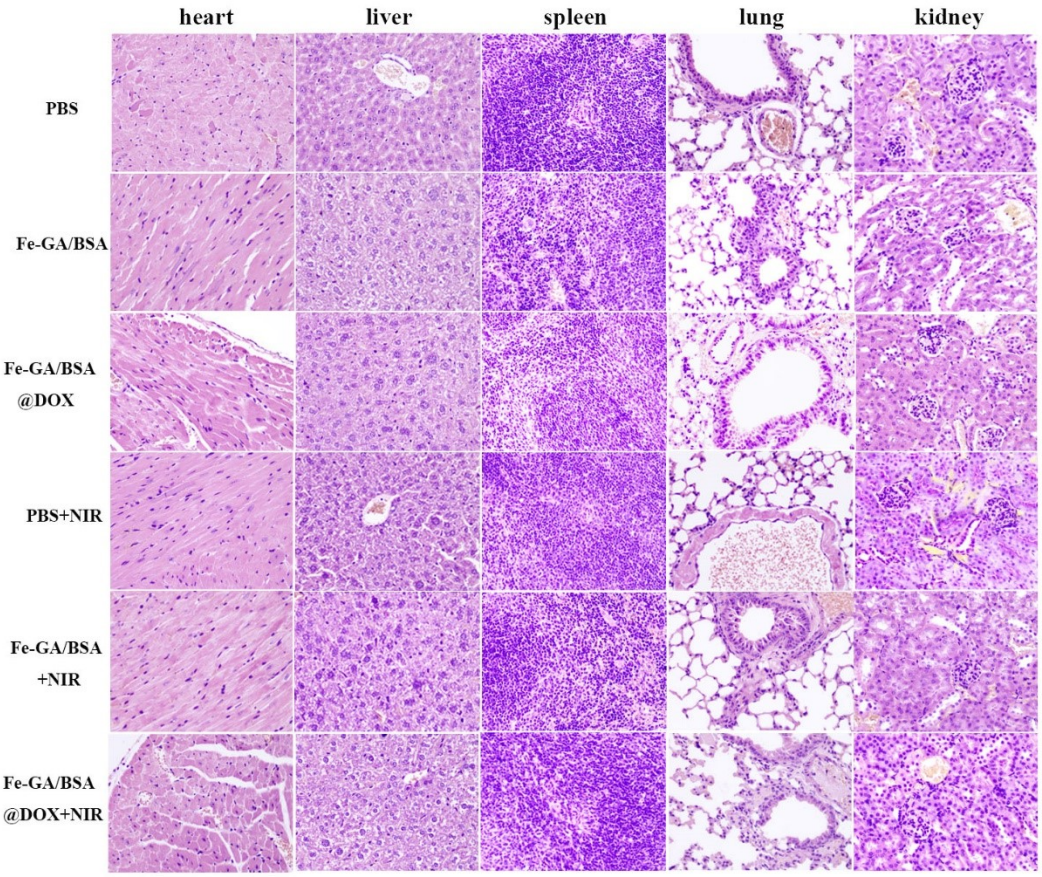


**Figure S10.** Tissue staining images of the main organs (heart, liver, spleen, lung, kidney) of tumor-bearing mice in different treatment groups

**References**

[1] Y. Liu, G. Yang, S. Jin, L. Xu and C.-X. Zhao, Development of High-Drug-Loading Nanoparticles, Chem Plus Chem, 2020,

[2] T. Zhang, Z. Jiang, L. Chen, C. Pan, S. Sun, C. Liu, Z. Li, W. Ren, A. Wu and P. Huang, PCN-Fe(III)-PTX nanoparticles for MRI guided high efficiency chemo-photodynamic therapy in pancreatic cancer through alleviating tumor hypoxia, Nano Research, 2020, 13, 273-281.

[3] G. Wang, D. Zhao, N. Li, X. Wang and Y. Ma, Drug-loaded poly +μ-caprolactone)/Fe 3 O 4 composite microspheres for magnetic resonance imaging and controlled drug delivery, Journal of Magnetism Magnetic Materials, 2018, 456, 316-323.

[4] X. Zhou, L. Jin, R. Q. Qi and T. Ma, pH-responsive polymeric micelles self-assembled from amphiphilic copolymer modified with lipid used as doxorubicin delivery carriers, Royal Society Open Science, 2018, 5

[5] J. Wang, H. Zhao, Z. Zhou, P. Zhou, Y. Yan, M. Wang, H. Yang, Y. Zhang, S. Yang, interfaces, MR/SPECT imaging guided photothermal therapy of tumor-targeting Fe@ Fe3O4 nanoparticles in vivo with low mononuclear phagocyte uptake, ACS applied materials, 8(31) (2016) 19872-19882.

[6] L.-S. Lin, Z.-X. Cong, J.-B. Cao, K.-M. Ke, Q.-L. Peng, J. Gao, H.-H. Yang, G. Liu, X. Chen, Multifunctional Fe3O4@ polydopamine core–shell nanocomposites for intracellular mRNA detection and imaging-guided photothermal therapy, ACS nano, 8(4) (2014) 3876-3883.

[7] Y. Liu, S. Liu, C. Hu, Y. Li, M. Pang, Facile synthesis of Fe-p-aminophenol nanoparticles for photothermal therapy, Dalton Transactions, 48(45) (2019) 16848-16852.

[8] Y. Wang, X. Liu, G. Deng, Q. Wang, L. Zhang, Q. Wang, J. Lu, Multifunctional PS@ CS@ Au–Fe 3 O 4–FA nanocomposites for CT, MR and fluorescence imaging guided targeted-photothermal therapy of cancer cells, Journal of Materials Chemistry B, 5(22) (2017) 4221-4232.

[9] Q. Tian, J. Hu, Y. Zhu, R. Zou, Z. Chen, S. Yang, R. Li, Q. Su, Y. Han, X. Liu, Sub-10 nm Fe3O4@ Cu2–xS core–shell nanoparticles for dual-modal imaging and photothermal therapy, Journal of the American Chemical Society, 135(23) (2013) 8571-8577.

[10] Y. Meng, J. Yang, R. Jiang, S. Wang, L. Zheng, G. Wang, X. Tian, H. Zhu, D. Yan, C. J. A. S. S. Liu, Biocompatible PLNP-GNR Composite Nanoplatforms for Monitoring Deep-tissue Photothermal Therapy Process, (2021) 150189.

[11] S. Zhou, X. Jiao, Y. Jiang, Y. Zhao, P. Xue, Y. Liu, J. J. A. S. S. Liu, Engineering Eu3+-incorporated MoS2 nanoflowers toward efficient photothermal/photodynamic combination therapy of breast cancer, 552 (2021) 149498.